Supplement of Atmos. Chem. Phys., 17, 11107–11133, 2017
https://doi.org/10.5194/acp-17-11107-2017-supplement

Atmospheric Chemistry and Physics
Open Access
EGU

Supplement of

Semivolatile POA and parameterized total combustion SOA in CMAQv5.2: impacts on source strength and partitioning

Benjamin N. Murphy et al.

Correspondence to: Benjamin N. Murphy (murphy.benjamin@epa.gov)

SVOC aging mechanism formulation

The theory of Donahue et al. (2012) was used both to determine the properties of the SVOC compounds used in this study and to populate the SVOC aging mechanism. The volatility of each surrogate species is calculated as a function of its given C^* and O:C. Specifically, we use the following relationship:

$$Log_{10}C^* = 0.475 * (25 - n_C) + 2.3 * n_O + 0.6 * n_C * n_O / (n_C + n_O) \quad \text{Eq. S1}$$

where C^* is the saturation concentration of the surrogate species in μg m^{-3}, n_C is the number of carbon atoms in the species, and n_O is the number of oxygen atoms in the species (Donahue et al., 2012).

Table S1 shows the stoichiometric coefficients derived from the branching ratio formula (Eq. 1) and the aging kernel published in Donahue et al. (2012). As an example, we provide the oxidation stoichiometry of the oxidation of VSVPO2, one of the surrogates for primary semivolatile vapors:

$$\begin{aligned} \text{VSVPO2} + \text{OH} \rightarrow \text{OH} &+ 0.3856 * \text{VLVPO1} + 0.0950 * \text{VSVPO1} \\ &+ 0.1373 * \text{VSVPO2} + 0.0005 * \text{VSVPO3} \\ &+ 0.2051 * \text{VLVOO1} + 0.1764 * \text{VLVOO2} \end{aligned} \quad \text{Eq. S2}$$

These molar yields are derived in order to conserve carbon. Hydroxyl radicals are assumed to be regenerated by the oxidation reactions so that the aging of POA does not perturb the oxidant budget; the overall reactivity associated with POA mass is small compared to that associated with VOCs. The stoichiometric coefficients indicate that low O:C surrogates (VLVPO1-VIVPO1) in addition to high O:C surrogates (VLVOO1-VSVOO3). This feature ensures that the evolution of bulk O:C behaves similarly to the more detailed approaches. This is described in more detail in the following section.

Box model analysis of SVOC aging mechanism

A box model was constructed to examine differences between the mechanism developed for this study (CMAQ52) and ones used in previous literature. The 2D-VBS formulation for low-NO_x conditions used by Chuang and Donahue (2016) was chosen for reference (REF). Alternative mechanisms included that of Koo et al. (2014) (KOO), Grieshop et al. (2009) (GRI), and the POA particle-phase aging mechanism found in CMAQv5.1 (Simon and Bhave, 2012) (CMAQ51). The CMAQ51 mechanism included nonvolatile POA but experienced mass growth as the particles age. The box model enforced a constant OH mixing ratio of 1 x 10^6 molec cm^{-3} and particles and vapors equilibrated between every time step (1 min). The initial OA (gas + particle = 10 μg m^{-3}) was given a volatility distribution equal to that of the primary emissions in CMAQv5.2, hence the semivolaitle configurations decrease dramatically in aerosol concentration in the first time step. A background concentratoin of 5 μg m^{-3} OA was assumed.

The CMAQ52 aging mechanism produced SOA at nearly the same rate as the REF mechanism for the first half hour at this loading and OH concentration (Fig. 1a). After an hour, the CMAQ52

underpredicts by about 10%, whereas the KOO case underpredicts throughout the time series. The GRI case produces SOA at the same rate as the KOO case for the first hour but then continues producing SOA, eventually overtaking the REF case. In general the SOA aging mechanism recovers to about 80% of the original POA mass concentration, and about 55% of the potential POA formed from oxidation. Similar relationships are seen at lower and higher initial concentrations and higher OH concentrations.

Figure 1b shows that the KOO and GRI do a better job predicting O:C of the REF case than does the CMAQ52 mechanism, which overpredicts by about 0.1 in O:C. This is a result of the relatively high O:C chosen for the oxygenated OA species. In the future, the model may treat this SOA production pathway with source-specific model species, allowing the O:C of those species to be more individually tailored to observations of that pollution source.

Tables S1. Molar yields specifying the product distribution of the photoxidation of primary organic vapors.

Reactant	VLVPO1	VSVPO1	VSVPO2	VSVPO3	VIVPO1	VLVOO1	VLVOO2	VSVOO1	VSVOO2	VSVOO3
VLVPO1	0.486	0.006	0.003	0.003	0.002	0.294	0.202	0.0	0.002	0.002
VSVPO1	0.300	0.286	0.004	0.004	0.0	0.224	0.182	0.0	0.0	0.0
VSVPO2	0.386	0.095	0.137	0.001	0.205	0.0	0.176	0.0	0.0	0.0
VSVPO3	0.218	0.306	0.015	0.104	0.0	0.189	0.167	0.0	0.0	0.0
VIVPO1	0.241	0.209	0.300	0.0	0.0	0.203	0.047	0.0	0.0	0.0
VLVOO1	0.0	0.0	0.0	0.0	0.0	0.666	0.014	0.012	0.124	0.183
VLVOO2	0.0	0.0	0.0	0.0	0.0	0.286	0.393	0.014	0.103	0.205
VSVOO1	0.0	0.0	0.0	0.0	0.0	0.330	0.227	0.261	0.070	0.112
VSVOO2	0.0	0.0	0.0	0.0	0.0	0.344	0.275	0.049	0.258	0.074
VSVOO3	0.0	0.0	0.0	0.0	0.0	0.389	0.242	0.064	0.039	0.267

Tables S2. Background CO values (ppbV) from observations and CMAQ predictions

Site	Observed	Reference	Predicted
Pasadena	110	Hayes et al. (2013)	85
Bakersfield	90	Gentner et al. (2012)	70
Cool	85	Setyan et al. (2012)	75

*Predicted background CO is calculated as the average of the bottom 5% of predicted CO concentrations.

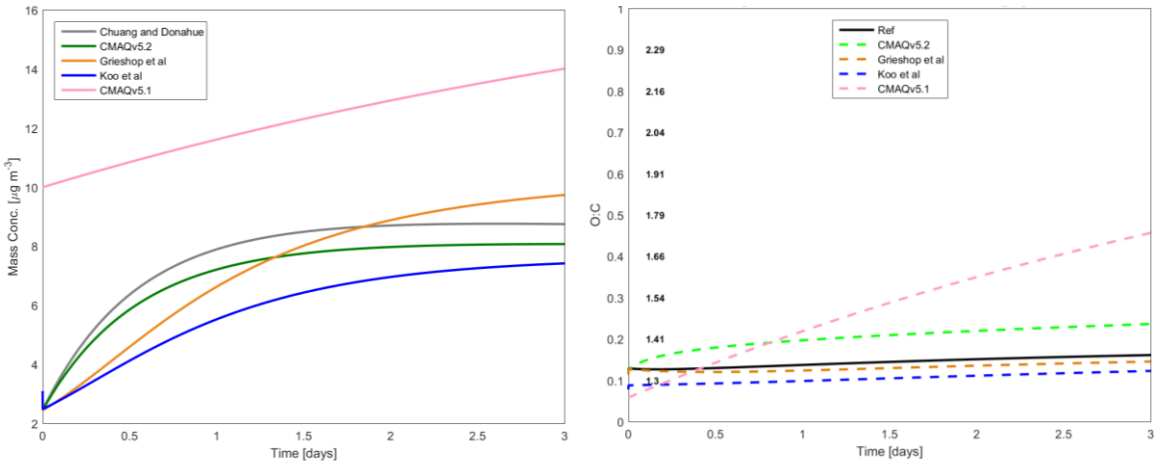

Figure S1. Box model OA concentrations (a) and O:C (b) with an assumed constant OH concentration equal to 1 x 10^6 molec cm^{-3}, an initial loading of 10 µg m^{-3} and a background OA concentration of 5 µg m^{-3}. In plot (b) the numbers on the inside of the left axis quanitfy OM:OC as a function of O:C using the method of Simon and Bhave (2012).

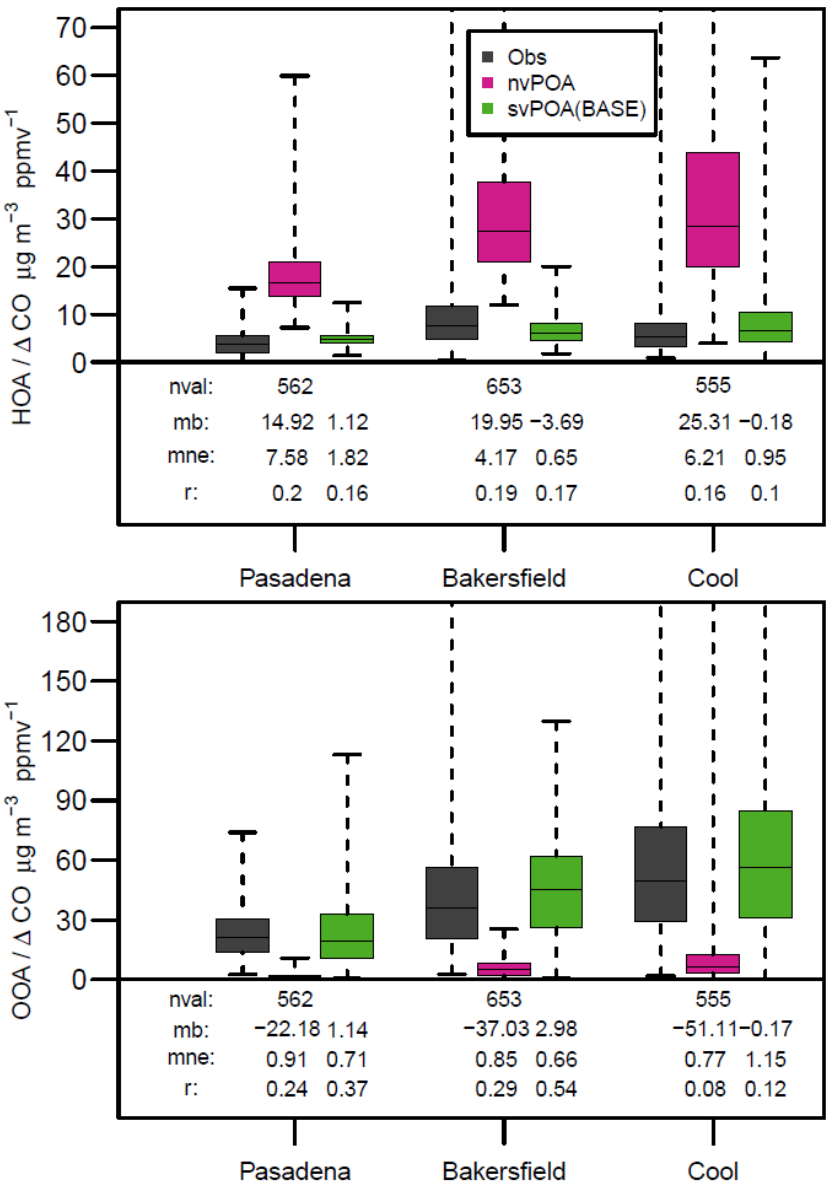

Figure S2. Evaluation of CMAQ-predicted hydrocarbon-like and oxygenated organic aerosol at 2 urban sites during CalNex (Pasadena and Bakersfield) and one urban downwind site during CARES (Cool). HOA and OOA from CMAQ are approximated by summing primary and secondary organic aerosol species, respectively, consistent with table 4. Here, all observed and predicted OA concentrations are normalized by the corresponding observed or predicted CO enhancement. The site-dependent background CO values applied to the observations are informed by existing literature while those applied to the CMAQ-predicted CO are calculated as the mean of the bottom 5% of the timeseries at each site. The background values are reported in table S2.

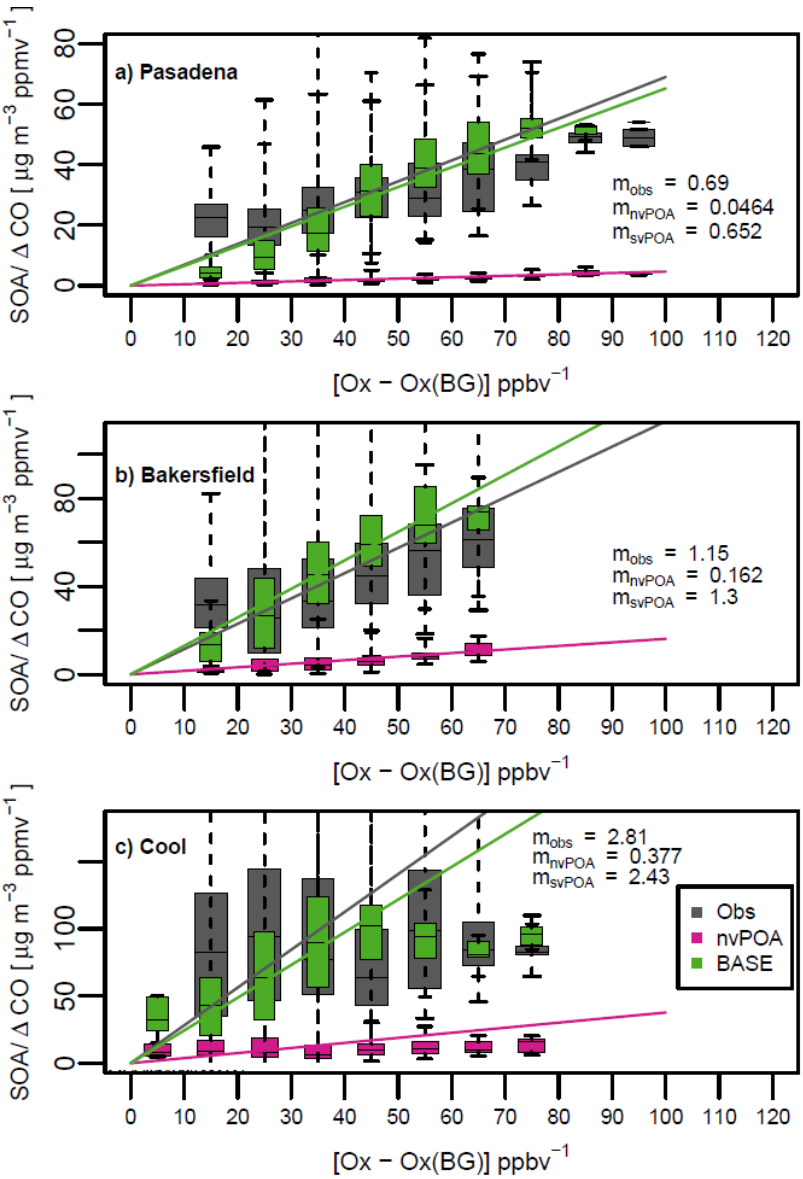

Figure S3. OOA observed and predicted enhancement as a function of oxidant loading at two urban sites during CalNex (Pasadena and Bakersfield) and one urban downwind sites during CARES (Cool). Ox concentrations are calculated as the sum of O_3 and NO_2 for Pasadena and Bakersfield. For Cool, the observed NO_2 concentrations are approximated as the difference between NO_y and NO. Here the OOA (observed) and SOA (predicted) concentrations are normalized by the CO enhancement (ΔCO) consistent with Fig. S2.

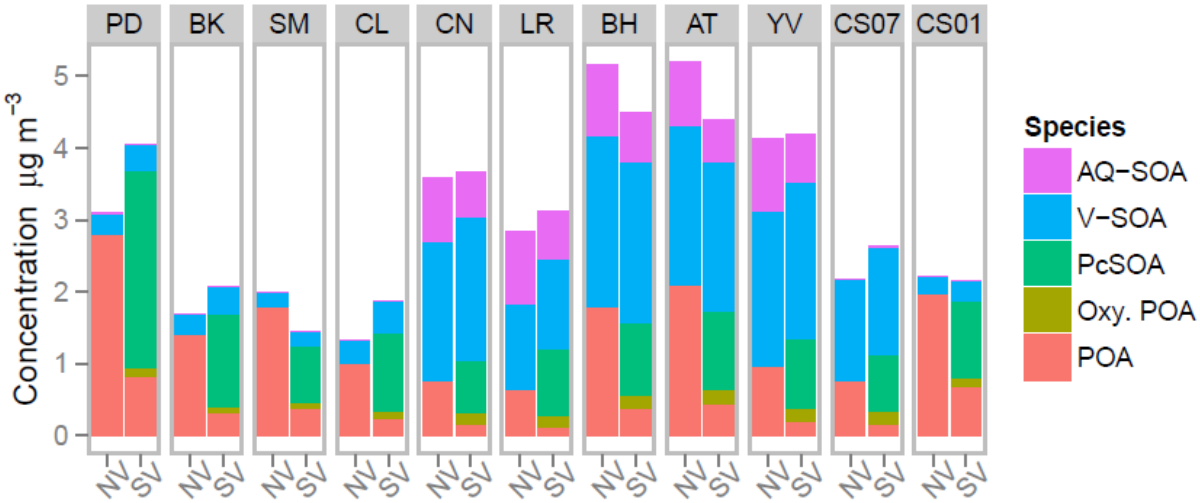

Figure S4. Composition of organic aerosol predicted by CMAQv5.2 run for both nonvolatile POA (NV) and semivolatile POA with pcSOA (SV). The species depicted include POA with very low O:C (POA), POA with high O:C (oxygenated POA or Oxy. POA), potential combustion SOA (pcSOA), SOA from traditional anthropogenic and biogenic VOCs (V-SOA), and SOA formed in the aqueous aerosol and cloud water phases (AQ-SOA). The sites shown in this figure include Pasadena (PD), Bakersfield (BK), Sacramento (SM), Cool (CL), Centreville (CN), Look Rock (LR), Birmingham (BH), Atlanta (AT), and Yorkville (YK). The rightmost two comparisons show the average contributions to OA for grid cells in the continental US from the CONUS11 simulation during July (CS07) and January (CS01). The higher contribution of AQ-SOA at the sites in the southeast US is a result of that simulation including isoprene and terpene aqueous-phase formation pathways that are not present in the California and CONUS-scale simulations.

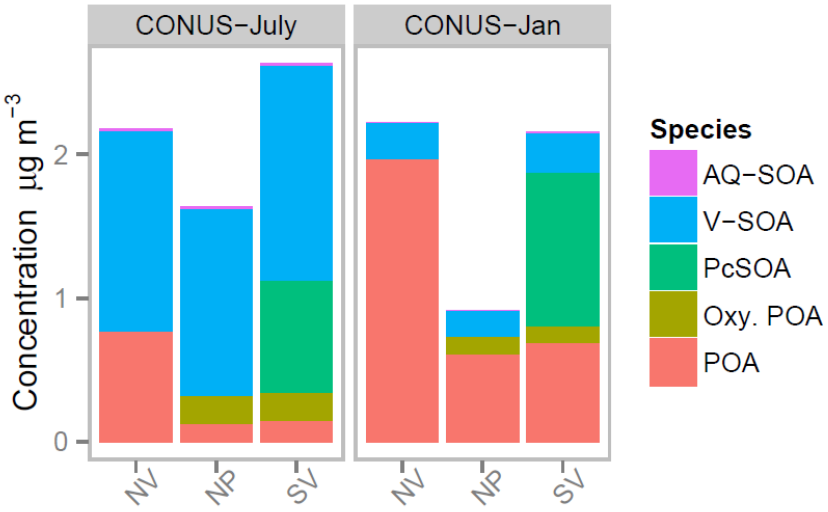

Figure S5. Composition of organic aerosol predicted by CMAQv5.2 run for both nonvolatile POA (NV), semivolatile POA with no pcSOA (NP), and semivolatile POA with pcSOA (SV). The species depicted include POA with very low O:C (POA), POA with high O:C (oxygenated POA or Oxy. POA), potential combustion SOA (pcSOA), SOA from traditional anthropogenic and biogenic VOCs (V-SOA), and SOA formed in the aqueous aerosol and cloud water phases (AQ-SOA). The concentrations are average contributions to OA for grid cells in the continental US from the CONUS11 simulation during July (CONUS-July) and January (CONUS-Jan).

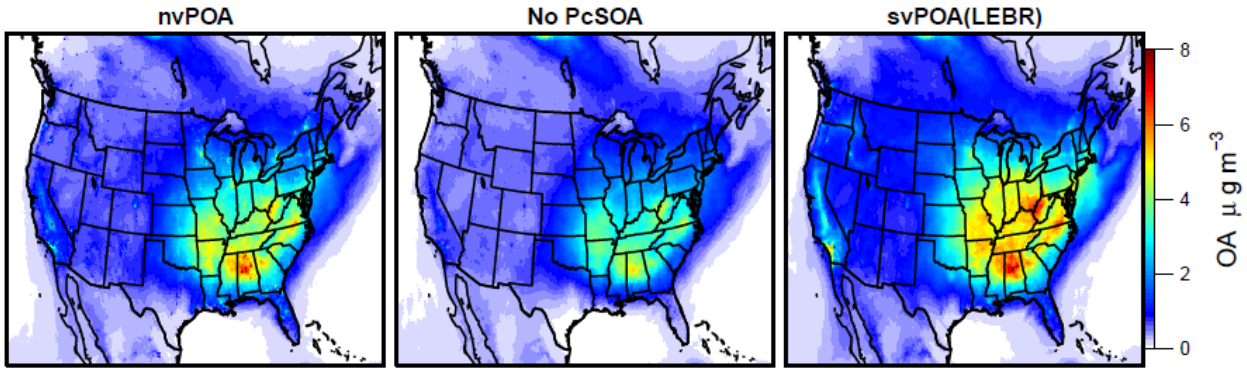

Figure S6. Average OA concentrations for nonvolatile POA (nvPOA), semivolatile POA with no pcSOA (No PcSOA), and semivolatile POA with pcSOA (svPOA(LEBR)). This simulation is for July, 2011.

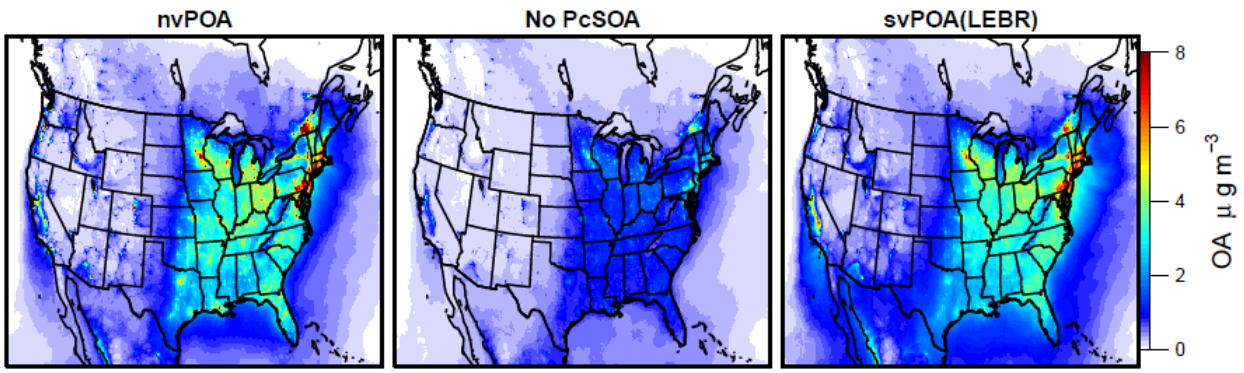

Figure S7. Average OA concentrations for nonvolatile POA (nvPOA), semivolatile POA with no pcSOA (No PcSOA), and semivolatile POA with pcSOA (svPOA(LEBR)). This simulation is for January, 2011.